Electro, Physical & Theoretical Chemistry

Stackable Aromatic Dipeptide Ring Structures toward Nanotube Formation: Thermodynamics and Interactions in Gas-Phase and Solution

Benjoe Rey B. Visayas and Maricris L. Mayes*[a]

Increasing attention has been drawn towards self-assembling dipeptide nanotube materials (NT) for their tunable properties. Despite recent advances, a fundamental understanding of the conditions that drive the self-assembly process is still lacking. Here, we report the structures, thermodynamics, and underlying interactions of the nanotube forming potential of cyclic and linear aromatic dipeptides phenylalanine-tyrosine, tryptophan-tyrosine, and dityrosine via the piecewise self-assembly mechanism. The cyclic dipeptides have better favorability of oligomerization in the gas phase than the linear dipeptides, largely due to the enthalpic gain of forming more hydrogen bonds, suggesting that the piecewise mechanism is plausible for vapor deposition methods. Oligomerization in solution, which would require desolvation of free monomers, was shown to be thermodynamically unfavorable, especially in polar solvents, demonstrating the need for an external stimulus for the crystallization of NTs. The generated oligomeric rings show structural robustness and symmetry, allowing excellent stacking potential in both lateral and axial directions. The nature of the sidechains significantly affects the stabilizations within the oligomeric structure. The insights generated can be used as a basis for dipeptide modifications that could enhance targeted NT properties for different applications.

1. Introduction

Interest in aromatic dipeptides has progressively increased over the last decade catalyzed by the work on diphenylalanine (FF), a core recognition motif of Alzheimer's β-amyloid (Aβ) polypeptide, which demonstrated self-assembly into discrete and extraordinarily stiff nanotubes (NTs).[1–3] The early works of Reches and Gazit reported hollow self-assembled FFNTs exhibiting exceptional stability and resistance from mechanical and chemical strains (e.g., heat, solvents, and enzymes),[4,5] leading to the development of FFNT with remarkable properties such as semi-conductor properties, photoluminescence, imaging, nanofluidics, and quantum dots, to cite a few.[6–10] FFNTs have also been explored for use in the biomedical field as biomimetic scaffolds, sensors, and drug delivery agents due to their relatively nontoxic properties.[11–13] Building on these advancements, current studies are looking at other possible protein-like NTs that can be formed from modified FF,[14] L/D amino acids,[15–17] and dipeptides from the combination of other aromatic amino acids tryptophan (W) and tyrosine (Y).[18–22]

The crystal structure of FFNTs has been well elucidated,[23–27] involving stacks of hexameric rings of FF in a head-to-tail conformation for intramolecular hydrogen bonding.[24,25,28] A single FFNT has an inner diameter of about 10 Å, while the bundles result in tubes with outer diameters ranging from 100–150 nm.[4,23,24] These FFNT crystals are traditionally prepared from a metastable gel-like phase by supplying an external stimulus to promote crystallization: temperature, liquid solvents, and, more recently, by gas-induced phase transition.[29–32] Solvent-less techniques such as plasma-enhanced chemical vapor deposition (PECVD) methods have also been used for synthesizing peptide NTs.[33,34]

Although the structure of FFNTs has been elucidated, the fundamental question of what drives the dipeptide nanostructure formation remains. To date, an accurate description of the energetics, even for the early stages, involved in the self-assembly process of dipeptide NTs is still lacking. Three prominent mechanisms are still in consideration for how dipeptide NT self-assembles: (1) rolling of two-dimensional dipeptide β-sheets into NTs,[35,36] (2) fusing of smaller spherical dipeptide vesicles into NTs,[37–39] and (3) piecewise formation of ring-like structures which then stack into NTs.[27,40] Moreover, conflicting observations are obtained even for the early stages of self-assembly. Based on molecular dynamics (MD) simulations, Tamamis et al.[41] suggested that hexameric rings are formed first, while Jeon et al.[28] suggested that the hydrophobic NT walls are formed first.

Previously, we studied the noncovalent interactions of tryptophan- and tyrosine-based dipeptide monomers and dimers.[18,19] In this paper, we present the results of extending the bottom-up approach beyond the dimeric size to investigate the stabilities and the underlying interaction energies of the dipeptide systems phenylalanine-tyrosine (FY), tryptophan-tyrosine (WY), and dityrosine (YY), in both their cyclic and linear forms. We provide insights into the thermodynamics of their

[a] B. R. B. Visayas, Prof. M. L. Mayes
Department of Chemistry and Biochemistry
University of Massachusetts Dartmouth
285 Old Westport Rd, North Dartmouth, MA 02747-2300, USA
E-mail: maricris.mayes@umassd.edu

Supporting information for this article is available on the WWW under https://doi.org/10.1002/slct.202102569

formation into oligomeric ring structures of quadmeric, pentameric, hexameric, and heptameric sizes, both in the gas phase and in solution, by quantifying their formation energies. Furthermore, we present the variation of formation energies and interaction energies (between individual monomers within the oligomeric ring structures) with respect to sidechain conformations. In addition, we provide insights into the need for external stimuli in NT formation in solution. Understanding the structures and thermodynamics of these oligomeric rings will provide insights into their potential stackability and whether a piecewise mechanism is plausible for these dipeptide systems.

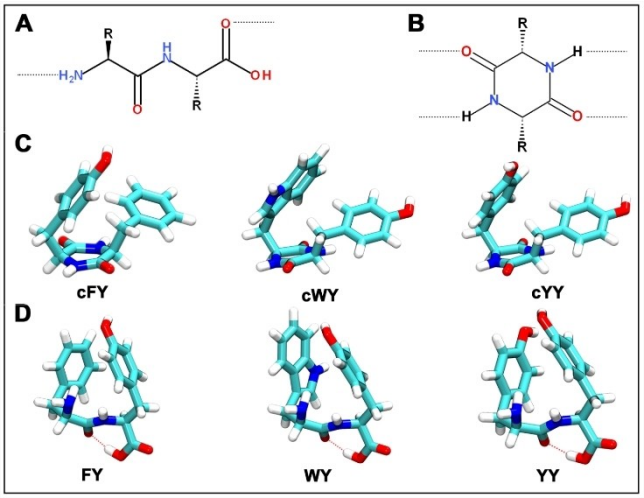

Figure 1. Structures of the (A) linear and (B) cyclic forms of LL dipeptides. The dashed lines represent the intermolecular interactions utilized in building the ring models. Molecular structures of the lowest-energy conformations of the FY, WY, and YY dipeptides in their cyclic (C) and linear (D) forms are also shown.

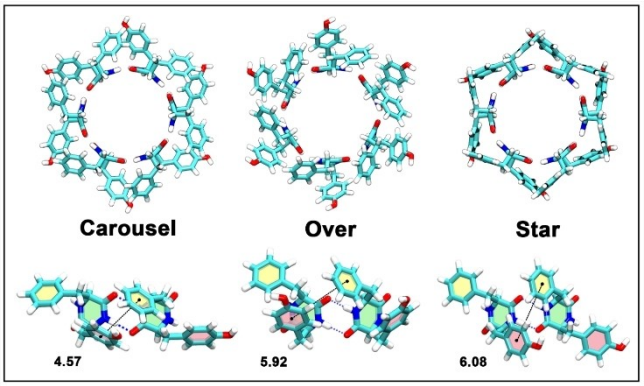

Figure 2. The three sidechain conformations considered in this study. Shown as an example is for cyclic FY (cFY) hexamer. Below each conformation are dimers extracted from the hexameric structure to show the sidechain orientations. Ring planes are shaded for clarity (yellow for F, red for Y, and green for the diketopiperazine ring). The distance between the centers of neighboring sidechains is also provided in Angstrom units. The carousel conformation is where the plane of the aromatic sidechains is perpendicular to the diketopiperazine ring. The over conformation is where the sidechains are directly above each other, which resembles the lowest-energy conformation of the monomer. Lastly, the star conformation is where the aromatic sidechains are parallel to the diketopiperazine ring.

2. Results and discussion

The possible quad-, penta-, hexa-, and heptameric ring structures formed from cyclic and linear FY, WY, and YY in the LL configuration were built by utilizing available H-bonding sites of either the peptide backbone (linear) or the diketopiperazine ring (cyclic). Figure 1 shows a schematic of these interaction sites for both the linear (Figure 1A) and cyclic (Figure 1B) forms of these dipeptides and the molecular structures of the lowest-energy conformations of the dipeptide monomers (Figures 1C and 1D). The H-bonded system served as the primary linkage between the monomers. We considered three sidechain orientations: carousel, over, and star. Figure 2 shows the geometries for the hexameric cyclic FY in these orientations. The "carousel" orientation is where the plane of the monomer sidechains is perpendicular to the diketopiperazine ring, which naturally imposes π- π interactions between the proximal sidechains of neighboring monomers. The "over" configuration utilizes the lowest-energy conformations of the dipeptide monomers where the sidechains are either angled up to nearly perpendicular (for cyclic dipeptides, Figure 1C) or almost parallel (for linear dipeptides, Figure 1D) with respect to each other. The "star" configuration is where the plane of the monomer sidechains is parallel to the diketopiperazine ring.

2.1. Dipeptide oligomeric ring structures

Stable oligomeric ring structures were obtained using the cyclic dipeptide monomers (cFY, cWY, cYY) and their linear counterparts (FY, WY, YY) in the carousel, over, and star conformations. Stability due to sidechain interactions and stability due to symmetry were two factors imposed in the conformations considered. The carousel conformation allows for maximum interactions between neighboring sidechains from hydrogen-bonding and π- π interactions. The star conformation maximizes the distance between neighboring sidechains but allows for a defined symmetry for the cyclic structure. The over-conformation uses the lowest energy conformation of the free dipeptide monomer. To illustrate these, Figure 2 shows the dimers extracted from the cyclic FY hexamers with the carousel conformation having the closest distance between the centers of neighboring sidechain rings at 4.57 Å.

Figure 3 (cFY), Figure 4 (cWY), Figure 5 (cYY), Figure 6 (FY), Figure 7 (WY), and Figure 8 (YY) show the corresponding optimized gas-phase geometries of the oligomeric ring structures. Also shown in these figures are the gas-phase free energy (ΔG, blue) and enthalpy (ΔH, green) in kcal/mol, relative to the over conformation, at the upper-right side as well as the pore diameter (black) and the number of hydrogen bonds (red; the first value shows the total number of hydrogen bonds, while the number in parenthesis is the number of intramolecular hydrogen bonds) at the lower-right side of each oligomeric structure. The pore diameter is measured as either the distance between the centers of the diketopiperazine rings

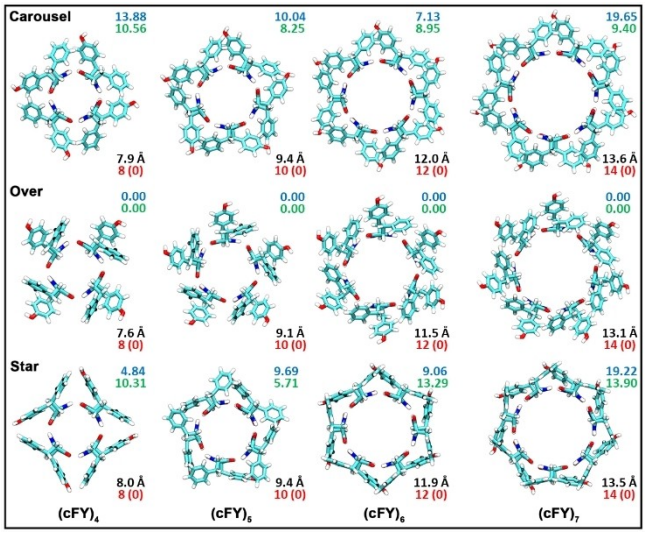

Figure 3. Licorice representation of the DFTB3-D3BJ optimized structures of the oligomeric rings of cyclic FY in the carousel, over, and star conformations. Free energy (ΔG, blue) and enthalpy (ΔH, green) in kcal/mol units relative to the over conformation, for each oligomeric size, are shown at the upper right of each structure. Also shown are the pore diameters (black) in Angstrom units and the number of hydrogen bonds (red; first value is the total number while the number in parenthesis is the number of intramolecular hydrogen bonds) at the lower right of each structure.

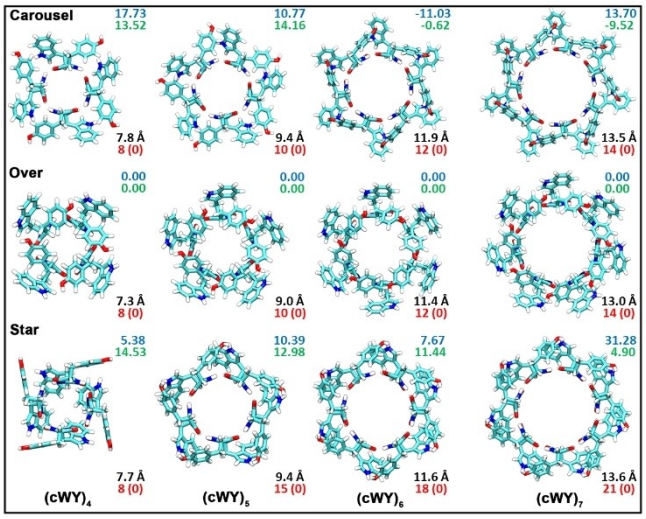

Figure 4. Licorice representation of the DFTB3-D3BJ optimized structures of the oligomeric rings of cyclic WY in the carousel, over, and star conformations. Free energy (ΔG, blue) and enthalpy (ΔH, green) in kcal/mol units relative to the over conformation, for each oligomeric size, are shown at the upper right of each structure. Also shown are the pore diameters (black) in Angstrom units and the number of hydrogen bonds (red; first value is the total number while the number in parenthesis is the number of intramolecular hydrogen bonds) at the lower right of each structure.

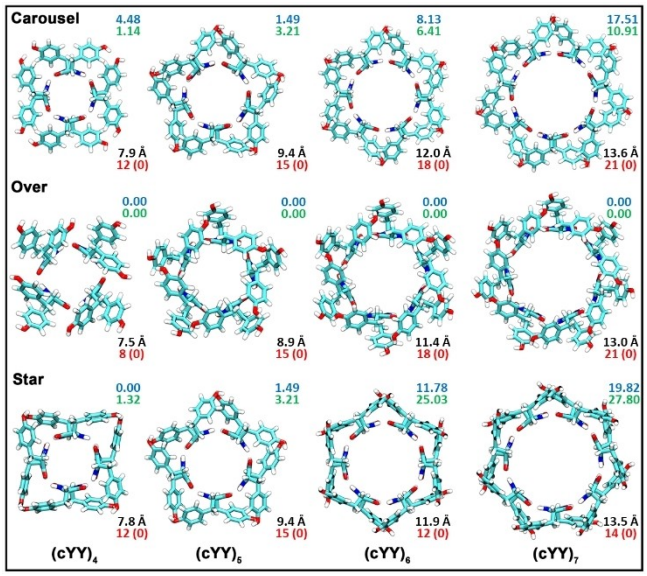

Figure 5. Licorice representation of the DFTB3-D3BJ optimized structures of the oligomeric rings of cyclic YY in the carousel, over, and star conformations. Free energy (ΔG, blue) and enthalpy (ΔH, green) in kcal/mol units relative to the over conformation, for each oligomeric size, are shown at the upper right of each structure. Also shown are the pore diameters (black) in Angstrom units and the number of hydrogen bonds (red; first value is the total number while the number in parenthesis is the number of intramolecular hydrogen bonds) at the lower right of each structure.

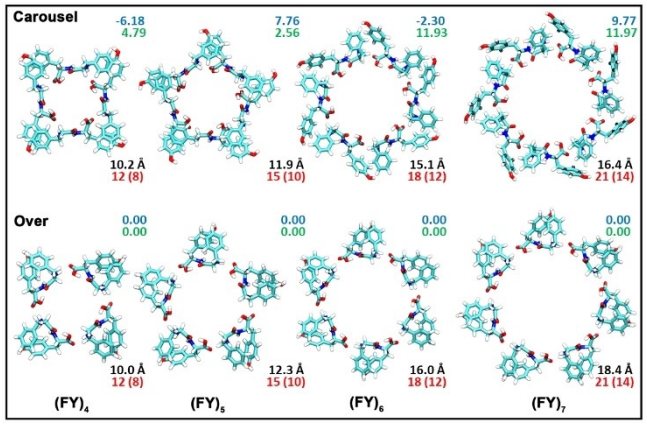

Figure 6. Licorice representation of the DFTB3-D3BJ optimized structures of the oligomeric rings of linear FY in the carousel and over conformations. Free energy (ΔG, blue) and enthalpy (ΔH, green) in kcal/mol units relative to the over conformation, for each oligomeric size, are shown at the upper right of each structure. Also shown are the pore diameters (black) in Angstrom units and the number of hydrogen bonds (red; first value is the total number while the number in parenthesis is the number of intramolecular hydrogen bonds) at the lower right of each structure.

for the cyclic dipeptides or the distance between the carbonyl carbons of the peptide bond for the linear dipeptides of two monomers opposite each other. A summary of the pore diameter and number of hydrogen bonds is also shown in Table S1. A defined ring pore is observed in all the oligomeric ring structures, consistent with the pore rings found in FF nanotubes. The diameter of these ring structures increases almost linearly as the oligomeric size increases (Figure 9). For the cyclic dipeptides, about a 2 Å increase is observed for each monomer added. The nature of the sidechains does not show a

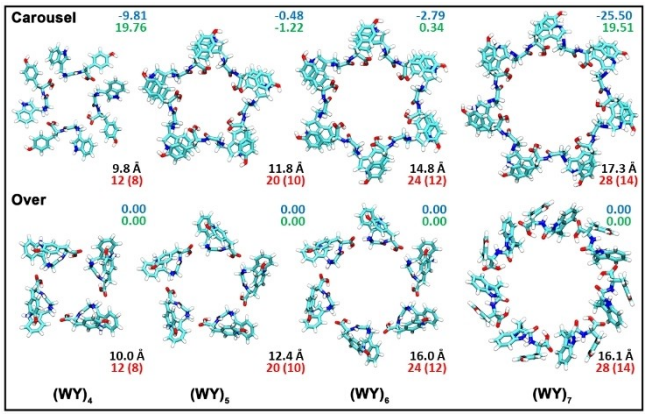

Figure 7. Licorice representation of the DFTB3-D3BJ optimized structures of the oligomeric rings of linear WY in the carousel and over conformations. Free energy (ΔG, blue) and enthalpy (ΔH, green) in kcal/mol units relative to the over conformation, for each oligomeric size, are shown at the upper right of each structure. Also shown are the pore diameters (black) in Angstrom units and the number of hydrogen bonds (red; first value is the total number while the number in parenthesis is the number of intramolecular hydrogen bonds) at the lower right of each structure.

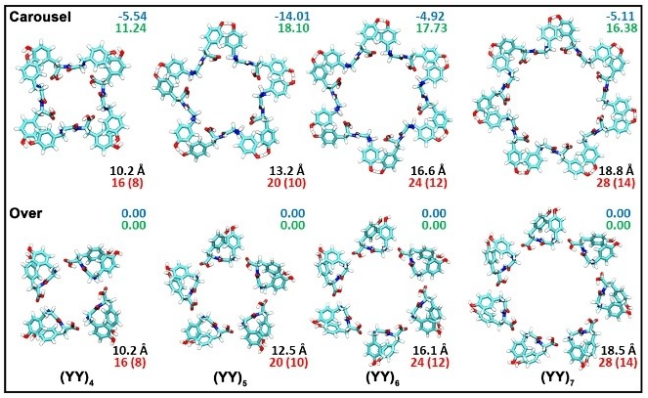

Figure 8. Licorice representation of the DFTB3-D3BJ optimized structures of the oligomeric rings of linear YY in the carousel and over conformations. Free energy (ΔG, blue) and enthalpy (ΔH, green) in kcal/mol units relative to the over conformation, for each oligomeric size, are shown at the upper right of each structure. Also shown are the pore diameters (black) in Angstrom units and the number of hydrogen bonds (red; first value is the total number while the number in parenthesis is the number of intramolecular hydrogen bonds) at the lower right of each structure.

significant effect on the pore diameter, and oligomers of cFY, cWY, and cYY have roughly the same diameters. However, the configuration type has an effect on the pore diameter. The carousel and star conformations have similar diameters and are systematically larger than the over conformations. This can be attributed to the steric effects of the sidechains in both the carousel and star conformations which push the monomers farther apart compared to the relatively more compact sidechains of the over conformation.

Moreover, the linear dipeptides have larger oligomeric ring structures than their cyclic counterparts due to the stretched-out peptide backbone compared to the more rigid diketopiperazine backbone. A similar systematic increase in the pore diameter is observed for the linear dipeptides, except for the WY heptamer in the over conformation, due to the puckering of the sidechains over the ring. Also, linear dipeptides allow better sidechain proximities, and consequently, better sidechain interactions.

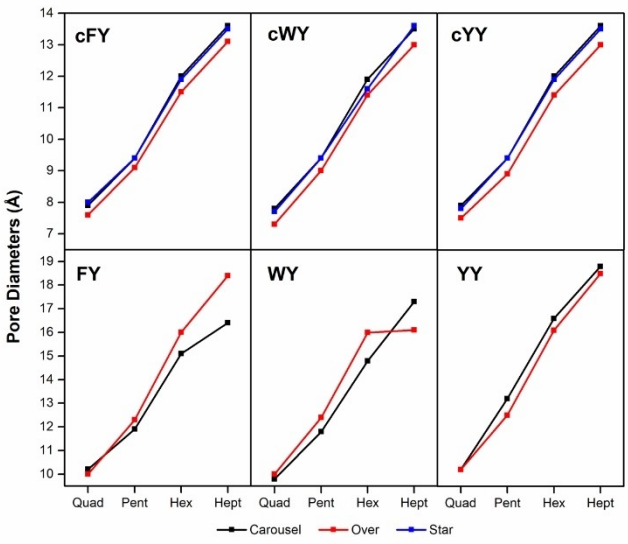

Figure 9. Pore diameters of the oligomeric structures.

Relative gas-phase free energies demonstrate that the over conformation is the preferred conformation in most cyclic dipeptide oligomers. The only exception is the hexameric cWY, where the carousel conformation is preferred. For the linear dipeptides, the carousel conformation is preferred except for the pentameric and heptameric FY.

2.2. Free energies of formation and solvation

In the gas phase, all three conformations considered for cyclic dipeptide oligomers are formed favorably, and generally become more favorable as the oligomeric size increases (Figure 10). This is primarily due to the enthalpic gain of the exothermic formation of the hydrogen-bonded pore ring structure as seen from the ΔH_f^{gas}(round symbols with dotted lines in Figure 10; data in Table S2). Contributions from sidechain interactions, particularly in the carousel conformations of cWY and cYY where both sidechains have polar characteristics, are also evident in the ΔH_f^{gas}. The entropic penalty of oligomerization, $-T\Delta S_f^{gas}$(triangular symbols with dashed lines), can also be inferred from Figure 10 and suggests that as the oligomeric size increases, the entropic penalty also increases and consequently reduces the favorability of oligomerization. This is particularly true for the carousel cWY, where there is a significant improvement in the ΔH_f^{gas} of the hexameric and heptameric rings. However, the entropic penalty makes the heptameric cWY less favorable than the hexamer. This could be a potential reason why the experimentally observed FF NTs have pore structures that are hexameric in nature.

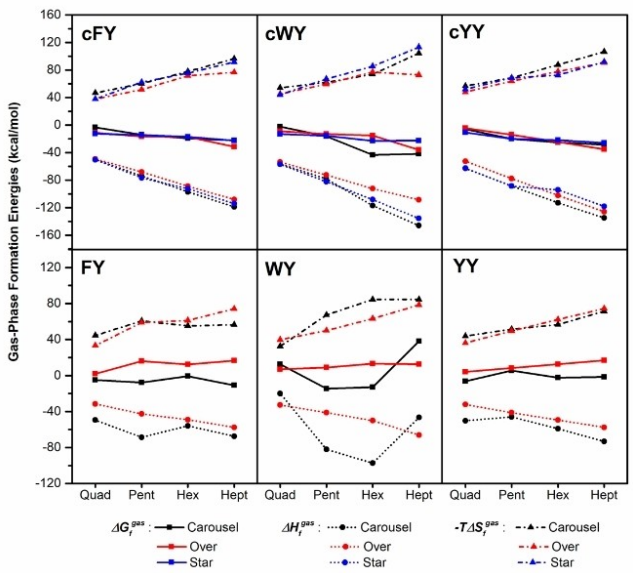

Figure 10. Calculated gas-phase free energies (ΔG_f^{gas}, box symbols and solid lines), enthalpies (ΔH_f^{gas}, round symbols and dotted lines), and entropies ($-T\Delta S_f^{gas}$, triangle symbols and dashed lines) of formation at 298 K. These formation energies were calculated from the corresponding total energy of the oligomer subtracted by the total energy of its comprising monomers.

On the other hand, the linear dipeptides are less spontaneous in their oligomerization than their cyclic counterparts. Only the carousel conformers show spontaneity of formation in the gas phase. The same trend is also observed here, where stabilization due to sidechain interactions promotes favorability for formation. As discussed before, the monomers' linear nature allows for better neighboring sidechain interactions, making the smaller oligomers more accessible. In the FY oligomers, the carousel pentamer and the heptamers are formed more favorably than the hexamer. In the WY oligomers, the pentamer and hexamer have roughly the same formation energy, while in YY, the hexamer shows to be the optimal size when comparing penta-, hexa-, and heptamers. The cyclic oligomers are more favorably formed in the gas phase than their linear counterparts. This is consistent with how peptide nanotubes are generally synthesized in vapor deposition methods, e.g., dehydrating linear dipeptides to form the cyclic forms or using the cyclic dipeptides as starting material.[33,40,42]

Table S3 shows a list of the solvation free energies of the oligomeric structures in water ($\varepsilon = 78.34$), acetone ($\varepsilon = 20.5$), and dichloromethane ($\varepsilon = 8.9$). Since the peptide backbone itself and the sidechains of the dipeptides considered in this study have polar ends, it is expected that the obtained solvation free energies are larger for polar solvents. Also, the proticity of the solvent shows a significant effect on the solvation, as evidenced by the huge difference between the solvation free energies in water to that of the solvation free energies in acetone and dichloromethane, which have roughly similar magnitudes. This is further demonstrated by the consistent difference between the solvation free energies of cFY and cYY as well as FY and YY, where each pair differs only by a single hydroxyl group.

Solvation considerably affected the formation of the oligomeric ring structures compared to the corresponding gas-phase formation (Figure 11A). In particular, for the cyclic dipeptide structures, a reversed trend is observed in the aqueous formation energies (Figure 11 B), while in the less polar aprotic solvents (Figure 11 C and D), the same general trend is observed, but with more positive formation energies compared to the gas-phase formation energies. On another hand, the linear dipeptides followed the same trend as the gas-phase trend but with more positive formation energy. Although this may be surprising at first, these results can be attributed to the fact that for these oligomeric structures to be formed in solution, free monomers, which are also solvated, must undergo desolvation to proceed with the oligomerization.[43,44] This explains the trend reversal in the aqueous formation energies of the cyclic dipeptides. Since the diketopiperazine ring pore structure utilizes all four hydrogen bonding sites (Figure 1B) for oligomerization, this would translate to a larger energy requirement in desolvating these sites of the monomer. This is more pronounced in water than the aprotic acetone and dichloromethane, where solvation effects on the formation energy are roughly similar. The linear oligomers do not suffer from this phenomenon as much as their cyclic counterparts since the linear oligomers utilize only two hydrogen bonding sites, which still leaves a free N–H for solvent interaction.

These oligomeric structures do not appear to favorably form in solution based on the solvated formation energies. This supports the suggestion that oligomerization to form the NT walls occurs first rather than the formation of pore rings in solution and that NT self-assembly is nucleation-driven. The thermodynamic unfavorability of these oligomerizations in solution also indicates the need for external stimulus. However, it is essential to note that solvent choice dramatically changes the thermodynamic profile, suggesting that solvent choice is a tweakable parameter in dipeptide NT self-assembly.

2.3. Monomer interaction energies within the oligomeric structure

To elucidate the types of interactions that govern the formation and stability of the dipeptide oligomers, we employed the PIEDA approach using the FMO2 framework, with MP2/6-31G* gas-phase energies. A monomer in each of the oligomeric structures was taken as a fragment, and its interaction energies towards the electrostatic field of the surrounding fragments were evaluated and categorized into exchange (E_{ex}), electrostatic (E_{es}), charge-transfer (E_{ct+mix}), and dispersion (E_{di}) component interactions. Figures 12 and 13 show the total and component interaction energies of the cyclic and linear dipeptides, respectively.

In general, as the oligomeric size increases, the total interaction energies are increasingly stabilizing for cyclic and linear dipeptide oligomers. But the star configurations of cFY and cYY hexamers have slightly lower total interaction energies (5 and 30 kcal/mol, respectively) compared to their pentameric

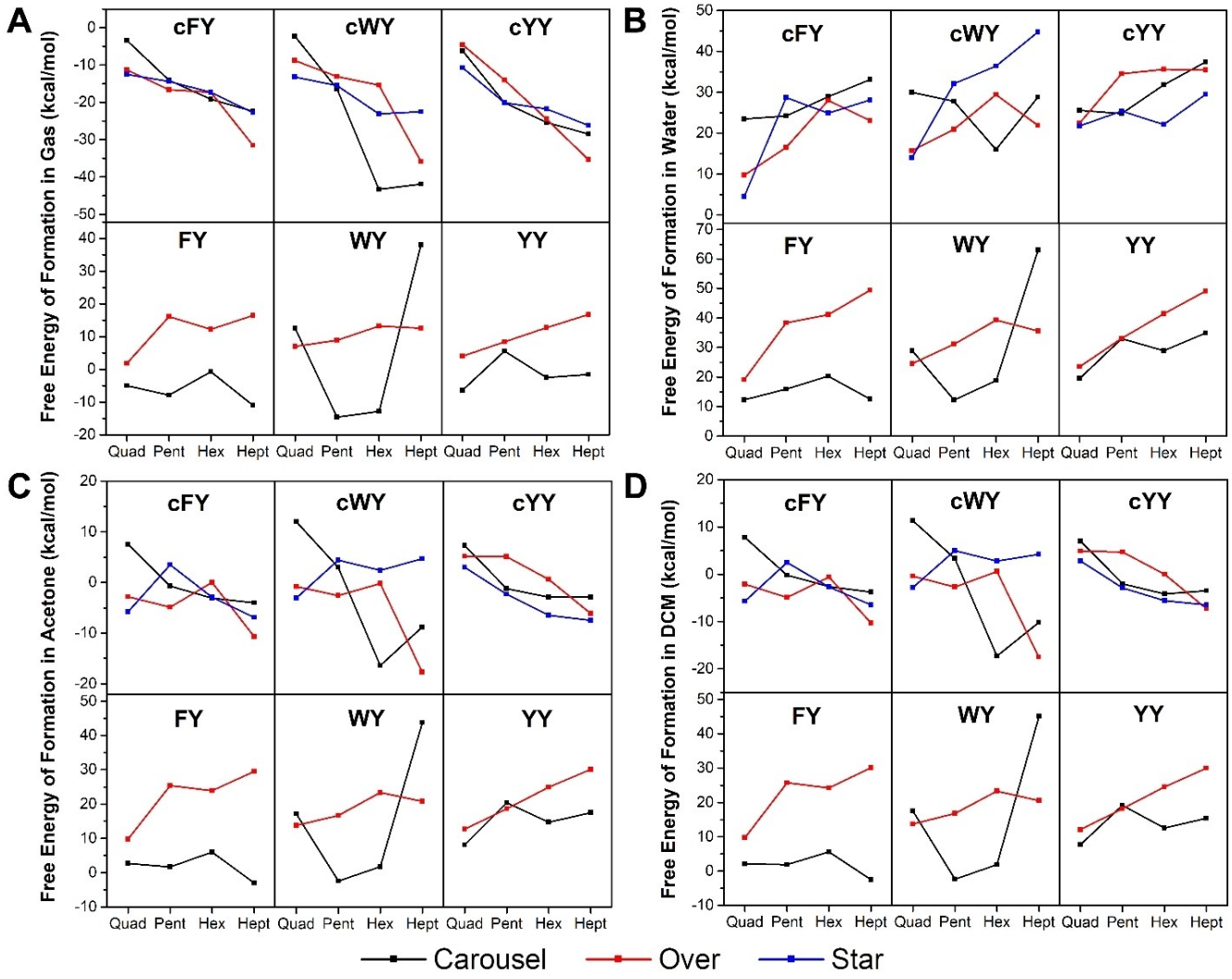

Figure 11. Calculated free energies of formation in gas (A), water (B), acetone (C), and dichloromethane (D) at 298 K. The formation energies are calculated from the total free energy of the oligomer subtracted by the total free energy of its comprising monomers.

counterparts. This discontinuity in the trend is attributed to the following geometrical constraints: the pentameric star cFY (Figure 3) allows for better electrostatic and dispersion interactions (Figure 12, right panel) due to the proximity of the tyrosine hydroxyl group towards the plane of the phenyl ring of phenylalanine which translates to a better stabilization compared to the hexameric star cFY. In contrast, the neighboring sidechain hydrogen bonding between tyrosine hydroxyl groups are lost in the hexameric and heptameric star cYY structures (Figure 5), which are available in the quadmeric and pentameric oligomers.

The cyclic dipeptide oligomers have about twice the stabilization from monomer interactions than their linear counterparts (−301 kcal/mol and −163 kcal/mol for cYY and YY heptamers, respectively). From the breakdown of the interaction energies of the dipeptide oligomers (right panels of Figures 12 and 13), it can be observed that the difference between the magnitudes of the total interaction energies of the cyclic and linear dipeptide oligomers is largely due to the electrostatic interactions (E_{es}). This is primarily attributed to the four hydrogen bonding pairs that comprise the diketopiperazine pore structure and the hydrogen bonding of the polar ends of the dipeptide sidechains. The dominant electrostatic interactions and the significant charge-transfer interactions (E_{ct+mix}) observed in the cyclic dipeptide oligomers could be rationalized as contributing factors to the conductive properties observed in dipeptide NTs.

Dispersion interactions provide a significant contribution as the oligomeric size is increased. This is especially true for the linear dipeptide oligomers, as their total interaction energies are largely comprised of dispersion rather than electrostatic interactions. Of the dipeptides considered, the cWY and WY exhibited the most benefit from the dispersion interactions, primarily due to the larger aromatic sidechain of W. As expected, the carousel conformations exhibited the most stabilization due to dispersion interactions, however, the over and star conformations of the cyclic dipeptide oligomers did exhibit surprisingly large dispersion interactions. This can be

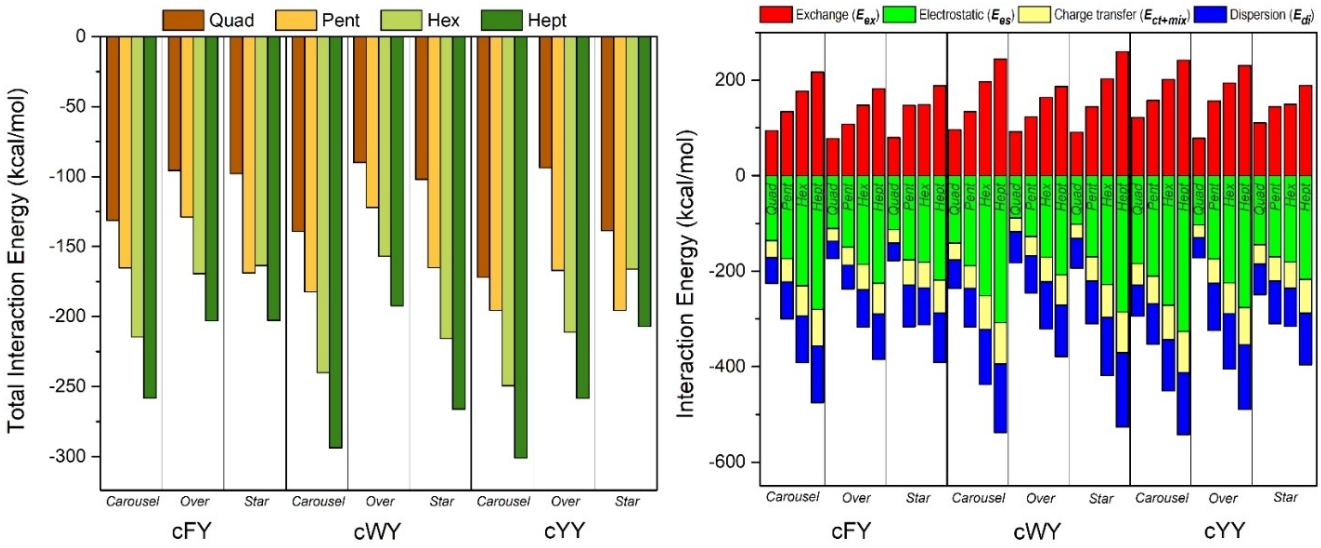

Figure 12. Total (left) and individual (right) interaction energies of the cyclic monomers for the different oligomeric structures from pair interaction energy decomposition analysis (PIEDA) using FMO-MP2/6-31G*.

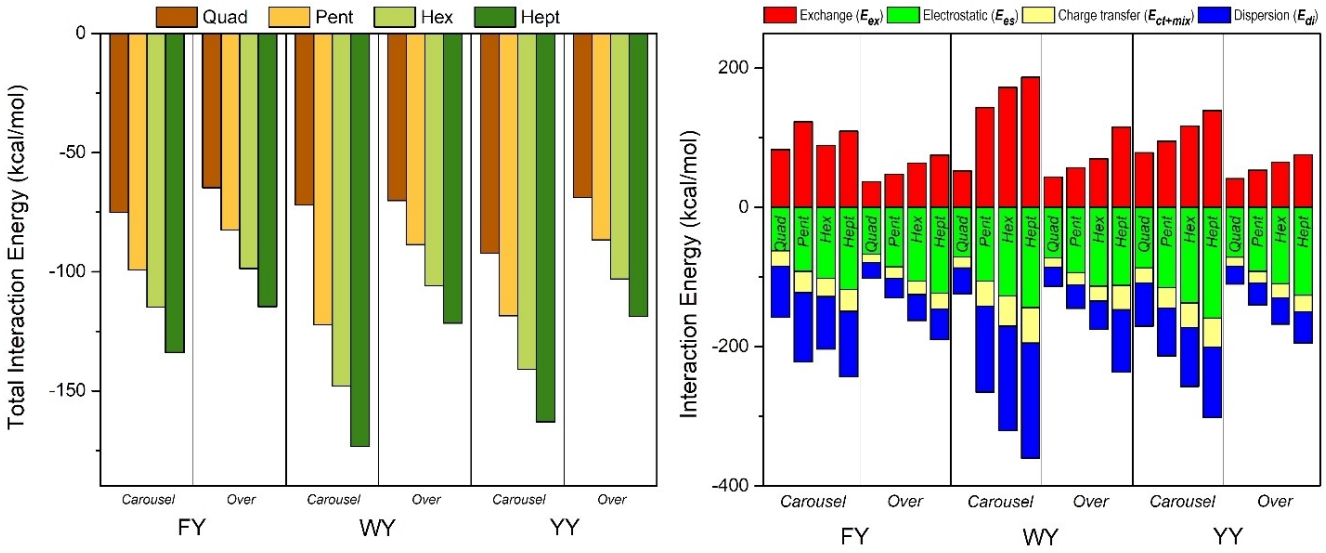

Figure 13. Total (left) and individual (right) interaction energies of the linear monomers for the different oligomeric structures from pair interaction energy decomposition analysis (PIEDA) using FMO-MP2/6-31G*.

attributed to the dispersion interactions of the sidechains in the over and star conformations towards the diketopiperazine ring itself, which induces a relatively minimal effect in the carousel conformation. The absence of the effect can be observed in the linear dipeptide oligomers, where the dispersion interactions are primarily due to sidechain interactions. There is a clear margin between the dispersion interactions of the carousel and the over conformations, with the carousel ones having the larger dispersion contributions to the total interaction energy.

We also looked at the average stability gained by an individual monomer from its interactions within the oligomeric structure (Figure 14). In almost all cases, the greatest stability from monomeric interactions is observed for the carousel conformation. Increased stability from oligomerization is also directly observable; as the oligomeric size increase, stability due to monomeric interactions also increases (more negative interaction energies), which is particularly true for the cyclic dipeptides.

Of the three conformations, the carousel has the most stabilizing interactions in all cases of oligomeric size (Figures 12 and 13) except for cFY pentamers, where the star has a slightly lower total interaction energy. To determine the effect of side chains on improving the interaction energy, we compared the

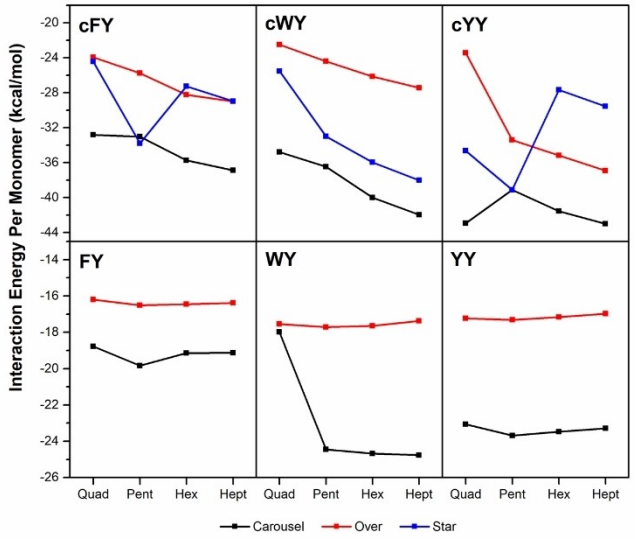

Figure 14. Average interaction energy per monomer of the oligomeric dipeptide ring structures.

average interaction energy per monomer of the dipeptide oligomers in Figure 14. It can be observed that functionalization of the aromatic sidechains (W and Y) considerably improved interactions in the carousels, i.e., interactions in WY and YY are more stabilizing than FY in both cyclic and linear cases. This could potentially translate to NTs with better mechanical and chemical properties than FFNTs.

3. Conclusions

This paper presented possible configurations of stackable oligomeric dipeptide ring structures of the aromatic FY, WY, and YY dipeptides in their cyclic and linear forms. Our results showed the favorable formation of these dipeptide oligomers in the gas phase making them viable for nanotube formation via vapor deposition methods. We also showed evidence of the thermodynamics of oligomerization in polar protic, polar aprotic, and nonpolar solvents, which support the need for external stimulus to promote crystallization as a consequence of monomer desolvation. Furthermore, we demonstrated that the formation of oligomeric rings in conformations that maximize sidechain interactions of neighboring dipeptide monomers, providing added stabilization for maintaining the ring structures, is the most preferred. Also, evidence of the different major contributing interaction types provides rationalization of the different potential properties of nanotubes formed from these dipeptides, i.e., cyclic dipeptides have significant charge-transfer and electrostatic interactions, making them potential semi-conductors. In contrast, linear dipeptides rely largely on dispersion interactions, potentially resulting in nanotubes with better mechanical properties. Finally, we demonstrated that the nature of the sidechains significantly affects the stabilizations within the oligomeric structure, where W and Y enhanced stabilization compared to F, which can lead to NT materials that have superior properties than FFNTs. Insights presented herein can be used as a basis for dipeptide modifications that could enhance targeted NT properties for different applications.

Supporting Information Summary

The associated Supporting Information includes details of the computational methodology implemented. Other supplementary data (pore diameters, number of hydrogen bonds, free energy components, and solvation energies) are also provided.

Acknowledgements

This research work was supported by the faculty research startup and Seed Funding program from the Office of the Provost at the University of Massachusetts Dartmouth. This research used the computing resources of UMass Dartmouth and the University of Massachusetts Green High Performance Computing Cluster.

Conflict of Interest

The authors declare no conflict of interest.

Keywords: aromatic dipeptides · cyclic peptides · density functional calculations · intermolecular interactions · oligomerization

[1] S. Brahmachari, Z. A. Arnon, A. Frydman-Marom, E. Gazit, L. Adler-Abramovich, *ACS Nano* **2017**, *11*, 5960–5969.
[2] E. Mayans, C. Alemán, *Molecules* **2020**, *25*, 6037.
[3] Lee, Trinh, Yoo, Shin, Lee, Kim, Hwang, Lim, Ryou, *Int. J. Mol. Sci.* **2019**, *20*, 5850.
[4] M. Reches, *Science* **2003**, *300*, 625–627.
[5] L. Adler-Abramovich, M. Reches, V. L. Sedman, S. Allen, S. J. B. B. Tendler, E. Gazit, *Langmuir* **2006**, *22*, 1313–1320.
[6] P. C. Saha, T. Bera, T. Chatterjee, J. Samanta, A. Sengupta, M. Bhattacharyya, S. Guha, *Bioconjugate Chem.* **2021**, *32*, 833–841.
[7] P. S. Zelenovskiy, E. M. Domingues, V. Slabov, S. Kopyl, V. L. Ugolkov, F. M. L. Figueiredo, A. L. Kholkin, *ACS Appl. Mater. Interfaces* **2020**, *12*, 27485–27492.
[8] N. Amdursky, M. Molotskii, D. Aronov, L. Adler-Abramovich, E. Gazit, G. Rosenman, *Nano Lett.* **2009**, *9*, 3111–3115.
[9] N. Amdursky, M. Molotskii, E. Gazit, G. Rosenman, *Appl. Phys. Lett.* **2009**, *94*, 261907.
[10] K. Tao, P. Makam, R. Aizen, E. Gazit, *Science* **2017**, *358*, DOI 10.1126/science.aam9756.
[11] B. Dinesh, M. A. Squillaci, C. Ménard-Moyon, P. Samorì, A. Bianco, *Nanoscale* **2015**, *7*, 15873–15879.
[12] T. Zohrabi, N. Habibi, A. Zarrabi, M. Fanaei, L. Y. Lee, *J. Biomed. Mater. Res. Part A* **2016**, *104*, 2280–2290.
[13] S. L. Porter, S. M. Coulter, S. Pentlavalli, G. Laverty, *Macromol. Biosci.* **2020**, *20*, DOI 10.1002/mabi.202000115.
[14] S. Kralj, O. Bellotto, E. Parisi, A. M. Garcia, D. Iglesias, S. Semeraro, C. Deganutti, P. D'Andrea, A. V. Vargiu, S. Geremia, R. De Zorzi, S. Marchesan, *ACS Nano* **2020**, *14*, 16951–16961.
[15] R. S. Giri, S. Pal, S. Roy, G. Dolai, S. R. Manne, S. Paul, B. Mandal, *Pept. Sci.* **2021**, *113*, e24176.
[16] S. Roy, R. S. Giri, G. Dolai, B. Mandal, *J. Mol. Struct.* **2020**, *1221*, 128877.
[17] Y. Wang, K. Wan, F. Pan, X. Zhu, Y. Jiang, H. Wang, Y. Chen, X. Shi, M. Liu, *Angew. Chem. Int. Ed.* **2021**, *60*, 16615–16621.
[18] M. L. Mayes, L. Perreault, *Comput. Theor. Chem.* **2018**, *1131*, 99–109.
[19] M. L. Mayes, L. Perreault, *ACS Omega* **2019**, *4*, 911–919.
[20] P. Macha, L. Perreault, Y. Hamedani, M. L. Mayes, M. C. Vasudev, *ACS Appl. Bio Mater.* **2018**, *1*, 1266–1275.

[21] D. G. Babar, S. Sarkar, *Appl. Nanosci.* **2017**, *7*, 101–107.
[22] J. Lee, M. Ju, O. H. Cho, Y. Kim, K. T. Nam, *Adv. Sci.* **2019**, *6*, 1801255.
[23] C. H. Görbitz, *Chem. Eur. J.* **2001**, *7*, 5153–5159.
[24] C. H. Görbitz, *Chem. Commun.* **2006**, *22*, 2332–2334.
[25] C. H. Görbitz, *Acta Crystallogr. Sect. B* **2010**, *66*, 84–93.
[26] T. Andrade-Filho, F. F. Ferreira, W. A. Alves, A. R. Rocha, *Phys. Chem. Chem. Phys.* **2013**, *15*, 7555.
[27] I. Azuri, L. Adler-Abramovich, E. Gazit, O. Hod, L. Kronik, *J. Am. Chem. Soc.* **2014**, *136*, 963–969.
[28] J. Jeon, C. E. Mills, M. S. Shell, *J. Phys. Chem. B* **2013**, *117*, 3935–3943.
[29] P. Zhu, X. Yan, Y. Su, Y. Yang, J. Li, *Chem. Eur. J.* **2010**, *16*, 3176–3183.
[30] T. Yuan, Y. Xu, J. Fei, H. Xue, X. Li, C. Wang, G. Fytas, J. Li, *Angew. Chem. Int. Ed.* **2019**, *58*, 11072–11077; *Angew. Chem.* **2019**, *131*, 11189–11194.
[31] P. Macha, M. L. Mayes, B. R. B. Visayas, V. Soni, V. R. Sammeta, M. C. Vasudev, *J. Mater. Chem. B* **2021**, *9*, 3900–3911.
[32] H. Xue, J. Fei, A. Wu, X. Xu, J. Li, *CCS Chem.* **2021**, *3*, 8–16.
[33] M. C. Vasudev, H. Koerner, K. M. Singh, B. P. Partlow, D. L. Kaplan, E. Gazit, T. J. Bunning, R. R. Naik, *Biomacromolecules* **2014**, *15*, 533–540.
[34] Y. Hamedani, P. Macha, T. J. Bunning, R. R. Naik, M. C. Vasudev, in *Chemical Vapor Deposition - Recent Advances and Applications in Optical, Solar Cells and Solid State Devices* (Ed.: S. Neralla), InTech, **2016**, 247–280.
[35] S. Guha, M. G. B. Drew, A. Banerjee, *Chem. Mater.* **2008**, *20*, 2282–2290.
[36] O.-S. Lee, S. I. Stupp, G. C. Schatz, *J. Am. Chem. Soc.* **2011**, *133*, 3677–3683.
[37] M. Rad-Malekshahi, L. Lempsink, M. Amidi, W. E. Hennink, E. Mastrobattista, *Bioconjugate Chem.* **2016**, *27*, 3–18.
[38] A. Rajbhandary, W. W. Brennessel, B. L. Nilsson, *Cryst. Growth Des.* **2018**, *18*, 623–632.
[39] N. Amdursky, M. Molotskii, E. Gazit, G. Rosenman, *J. Am. Chem. Soc.* **2010**, *132*, 15632–15636.
[40] L. Adler-Abramovich, E. Gazit, *Chem. Soc. Rev.* **2014**, *43*, 6881–6893.
[41] P. Tamamis, L. Adler-Abramovich, M. Reches, K. Marshall, P. Sikorski, L. Serpell, E. Gazit, G. Archontis, *Biophys. J.* **2009**, *96*, 5020–5029.
[42] B. Bank-Srour, P. Becker, L. Krasovitsky, A. Gladkikh, Y. Rosenberg, Z. Barkay, G. Rosenman, *Polym. J.* **2013**, *45*, 494–503.
[43] K. Kanagaraj, M. Alagesan, Y. Inoue, C. Yang, in *Comprehensive Supramolecular Chemistry II*, Elsevier, **2017**, 11–60.
[44] X. Pan, C. E. Glatz, *Cryst. Growth Des.* **2002**, *2*, 45–50.

Submitted: July 21, 2021
Accepted: October 12, 2021